



Cite this: DOI: 10.1039/d2cc05876f

 Received 29th October 2022,
Accepted 7th December 2022

DOI: 10.1039/d2cc05876f

rsc.li/chemcomm

Real-space visualization of sequential debromination of polybrominated benzenes on Ag(111)[†]

 Lina Shang, Wenze Gao, Faming Kang, Zhaoyu Zhang, Chi Zhang* and Wei Xu *

By a combination of scanning tunneling microscopy imaging and density functional theory calculations, dehalogenation processes of symmetric polyhalogenated benzenes were explored on Ag(111), and a series of intermediate states were captured and visualized in real space. These results reveal a sequential dehalogenation scenario of symmetric polybrominated aromatics, which will broaden the understanding of on-surface dehalogenation reactions.

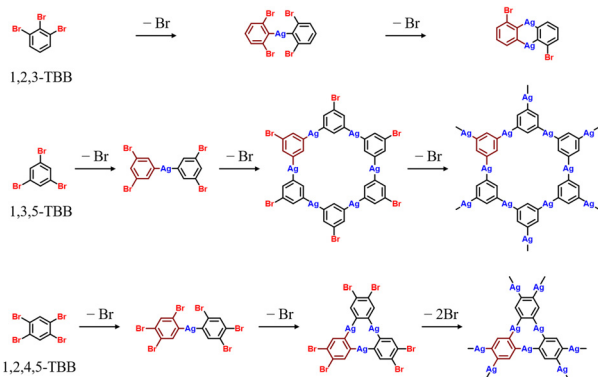
Dehalogenation reaction, which involves the cleavage of C–X bonds (X stands for halogen), has been appealing in organic chemistry with potential in the detoxification and fabrication of pharmaceutical drugs.¹ It has also attracted great attention from the surface science community as a versatile strategy to construct C–C bonds and corresponding carbon-based nanoarchitectures *via* on-surface synthesis.² Moreover, by means of *in situ* characterization techniques, such as scanning tunneling microscopy (STM) and atomic force microscopy (AFM),³ sets of intermediates, generally classified into surface-stabilized radicals and organometallic intermediates, have been successfully captured on surfaces and visualized in real space,^{4–6} which is usually a great challenge in traditional organic synthetic chemistry. As early as 2000, Hla *et al.* reported deiodination and sequential coupling processes (*i.e.*, Ullmann reaction) on surface with all elementary steps controllably triggered by STM tip manipulations and intermediates captured.⁷ Since then, Ullmann-type dehalogenation reactions have been extensively investigated on surfaces for the construction of various π -conjugated nanostructures typically like graphene nanoribbons^{8,9} and non-benzenoid carbon allotropes¹⁰ for applications in molecular electronics. Interestingly, organometallic nanostructures with C–M–C connections (M: metal) involved in the dehalogenation reaction pathways also have

potential in electronic devices and nanocircuits due to their high electron transport through metal–organic junctions.^{5,11} To regulate the target nanostructures and reaction pathways of dehalogenation reactions, catalytic substrates,¹² kinetics,^{13,14} thermodynamics,^{13,15} and molecular precursors^{16,17} have been subtly modified and controlled. The influence of substituents at different sites,¹⁸ closely related to the precursor design, has also been extensively investigated in previous reports, where substituents could affect the dehalogenation sequence¹⁹ as well as the reactivity of adjacent sites.²⁰ Moreover, distinct interaction with the substrate can greatly affect the activation sequence of symmetric sites through manipulation and thermal activation on surfaces.^{6,21} Recently, debromination reactions of typical linear molecules with *para*-substitution^{22,23} have been explored, showing dissymmetric debromination processes on surfaces. In addition, the dehalogenation of polyhalogenated aromatics has been theoretically studied,²⁴ where bromines located at the same sites of benzenes were calculated to have the same dissociation energy of the C–Br bond. However, multiple substitutions on a single benzene (such as halogen substitution *ortho*, *meta*, and *para*) forming symmetric molecular precursors have not been experimentally explored to the best of our knowledge, and the corresponding dehalogenation reaction processes have not been fully understood. It is therefore of fundamental interest to explore the dehalogenation processes of these typical symmetric polyhalogenated benzenes (which have multiple C–Br bonds in the same chemical environment) and monitor their individual intermediate states on surfaces.

In this study, three symmetric polyhalogenated aromatics were selected as molecular precursors, *i.e.*, 1,2,3- and 1,3,5-tribromobenzenes, and 1,2,4,5-tetrabromobenzenes (shortened as 1,2,3-TBB, 1,3,5-TBB, and 1,2,4,5-TBB, *cf.* Scheme 1), to investigate their debromination behaviors on Ag(111). By a combination of STM imaging and DFT calculations, sets of unique stable organometallic intermediates were captured during debromination and visualized in real space, revealing sequential dehalogenation processes of symmetric polyhalogenated aromatics. 1,2,3-TBB belonging to the C_{2v} point group

Interdisciplinary Materials Research Center, College of Materials Science and Engineering, Tongji University, Shanghai 201804, People's Republic of China.
E-mail: xuwei@tongji.edu.cn, zhangchi11@tongji.edu.cn

[†] Electronic supplementary information (ESI) available. See DOI: <https://doi.org/10.1039/d2cc05876f>



Scheme 1 Schematic illustration showing sequential debromination processes of 1,2,3-TBB, 1,3,5-TBB, and 1,2,4,5-TBB on Ag(111). The number of dissociated bromines is designated for each molecular precursor.

(with one C_2 axis) was firstly applied to investigate the debromination sequence of three adjacent C–Br bonds, where the central one was predicted to be the weakest,²⁴ and this resulted in the stepwise generation of zero-dimensional (0D) organometallic motifs. By further using equally distributed tribromo-substituents (that is, 1,3,5-TBB belonging to C_{3h} point group with three C_2 axes), a sequential evolution from 0D organometallic dimers, through hexamers, to 2D honeycomb-like frameworks was observed on Ag(111) upon debromination. Furthermore, functionalization of the benzene with more bromo-substituents, *i.e.*, 1,2,4,5-TBB belonging to the C_{2h} point group with two C_2 axes, led to the formation of 2D organometallic networks with more Ag adatoms integrated into the connections. During debromination, 1,2,4,5-TBB underwent transformation to organometallic dimers, trimers, and networks. Thus, sequential dehalogenation processes of three symmetric polybrominated benzenes were visualized, providing experimental understandings of the activation processes of multiple equivalent reaction sites within polyhalogenated aromatics, which would further expand the database of dehalogenation reactions as well as provide strategies for the bottom-up fabrication of nanostructures.

As the first step, 1,2,3-TBB with a C_2 axis was applied to visualize the debromination process on Ag(111). After deposition onto a cold substrate held at ~ 120 K, intact 1,2,3-TBB monomers were observed. From the large-scale STM image (Fig. S1a, ESI[†]), isolated ones could be identified in a cat-claw shape as typically depicted in Fig. 1a. Three protrusions adjoining each other are assigned to three adjacent Br atoms, while the remaining big one is a phenyl ring, in agreement with the STM simulation on Ag(111) (*cf.* Fig. 1d and Fig. S2, ESI[†]). Furthermore, when 1,2,3-TBB was deposited at ~ 220 K, dimer-like motifs with bright centers appeared (Fig. S1b, ESI[†]). Close inspection revealed the morphology of two cat-claw shapes sharing one bright protrusion (Fig. 1b), which was attributed to an organometallic dimer from DFT calculations (Fig. 1e). The central Br atom is eliminated with the formation of a C–Ag–C bond, leading to the generation of an organometallic dimer, and the Ag connection appears as a bright

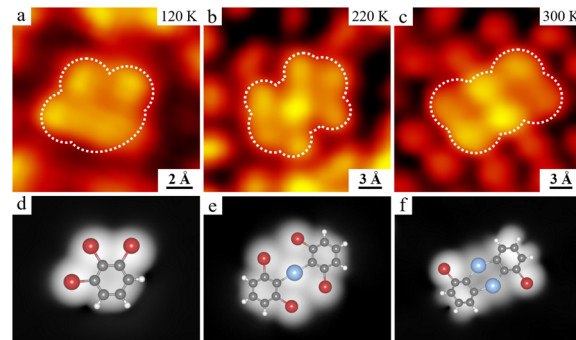


Fig. 1 Sequential debromination of 1,2,3-TBB on Ag(111). (a) High-resolution STM image of the intact monomer after deposition of 1,2,3-TBB onto Ag(111) held at ~ 120 K. (b and c) Organometallic dimers obtained by depositing 1,2,3-TBB onto Ag(111) at ~ 220 K and ~ 300 K, respectively. The individual motifs are indicated by white contours. Typical scanning conditions: $V_t = -750$ mV, $I_t = 1.20$ nA. (d–f) Simulated STM images of (d) an intact monomer and (e and f) two kinds of organometallic dimers superimposed with the corresponding DFT-optimized models. Gray: C; red: Br; blue: Ag; white: H.

protrusion. Note that the middle C–Br bond (at C_2 site) was theoretically predicted to have a lower dissociation enthalpy²⁴ compared to the others due to the adjacent C–Br bond and high steric interactions, which agrees well with the sequential debromination process observed in our experiment. Interestingly, when 1,2,3-TBB was deposited at 300 K, bowknot-shaped dimers appeared with two protrusions located at the center (Fig. 1c and Fig. S1c, ESI[†]). According to DFT calculations (Fig. S2, ESI[†]), the central protrusions are assigned to Ag atoms connecting two molecular components at the *ortho*-region, indicating that two metal atoms are integrated into the organometallic dimer (Fig. 1f). It also indicates that two Br atoms in the same chemical environment tend to dissociate step by step on the surface. After further annealing the sample at higher temperatures, disordered motifs were obtained due to the complicated substituent positions. Therefore, a sequential debromination process in 0D was captured by visualizing the organometallic intermediates involved.

To explore the dehalogenation process based on equally distributed bromo-substituents, 1,3,5-TBB molecules (with three C_2 axes) were sublimed onto Ag(111) at 300 K and formed two different phases with an obvious boundary (Fig. S3, ESI[†]). The high-resolution STM image showed that one is a close-packed array of intact monomers (Fig. 2a). The corresponding zoomed-in STM image (Fig. 2e) clearly shows the arrangement within the molecular islands, where both isolated 1,3,5-TBB molecules and trimers formed by three intact molecules *via* halogen bonds^{25,26} can be found and are depicted by blue contours of triangular darts. 1,3,5-Br substituents appear as bright dots at the three termini, which agrees well with the STM morphology (see the superimposed structural models). In addition, an ordered yet distinct self-assembled phase was also observed (Fig. 2b). From the close-up STM image (Fig. 2f), dogbone-shaped structures with bright central dots could be identified and were surrounded by dissociated Br atoms²⁷

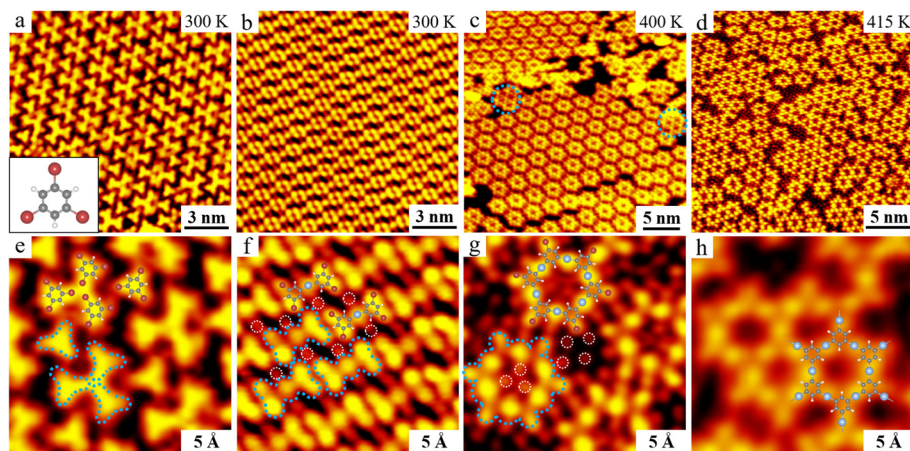


Fig. 2 Sequential debromination of 1,3,5-TBB on Ag(111). (a and b) Large-scale STM images of self-assembled (a) intact 1,3,5-TBB monomers (with DFT-optimized model shown at the bottom left), and (b) organometallic dimers on Ag(111) upon deposition at 300 K. (c and d) Large-scale STM images of (c) hexamers and (d) 2D networks on Ag(111) obtained after annealing the sample at ~ 400 K and ~ 415 K, respectively. (e–h) The corresponding close-up STM images of (e) monomers, (f) dimers, (g) hexamers, and (h) networks with structural models superimposed, where individual motifs are depicted by blue contours. White dotted circles indicate dissociated bromine atoms. Typical scanning conditions: $V_t = -880$ mV, $I_t = 1.10$ nA.

(depicted by white dotted circles). Based on the situation of 1,2,3-TBB shown above, previous reports,^{13,28} and DFT calculations, the dogbone-shaped structure is attributed to an organometallic dimer with a C–Ag–C connection (Fig. 2f). Notably, different from the reported situation of 1,3,5-TBB adsorbed on Cu(111),²⁸ where organometallic networks were uniformly formed, a stepwise evolution of organometallic intermediates was captured on Ag(111). After further annealing the above sample at 400 K for 30 mins, large islands of hexagonal rings formed (Fig. 2c) (with a starting temperature at 360 K) as a result of further debromination. An individual hexamer is depicted by a blue contour in Fig. 2g, with the corresponding DFT-optimized model overlaid. The six bright dots within each ring are revealed to be Ag atoms incorporated in the organometallic hexamer, while the remaining Br atoms within molecular components are located at the six termini. Besides, some dark red dots as highlighted in white circles are assigned to the dissociated bromine atoms.²⁹ Meanwhile, small patches of organometallic networks started to form as indicated by blue circles. Furthermore, more complete debromination took place at ~ 415 K, leading to the appearance of honeycomb-like organometallic networks (Fig. 2d). Comparison between the close-up high-resolution STM images of Fig. 2g and h indicates that further debromination occurred at the periphery of the hexagonal rings, leading to connections among the hexamers. The statistics of the proportion of doubly- and triply-dehalogenated 1,3,5-TBB are shown in Fig. S4 (ESI[†]). Note that owing to the surrounding Br atoms as obstacles, further growth into larger organometallic networks of high quality was prohibited.²⁷

As the next step, more halogen substituents are involved to examine whether such sequential debromination processes also occur, and a symmetric 1,2,4,5-TBB molecule (with two C_2 axes) was investigated. Fig. 3a shows a typical STM image of well-ordered islands assembled by intact monomers after deposition onto Ag(111) held at ~ 140 K. Thereafter, annealing the sample at

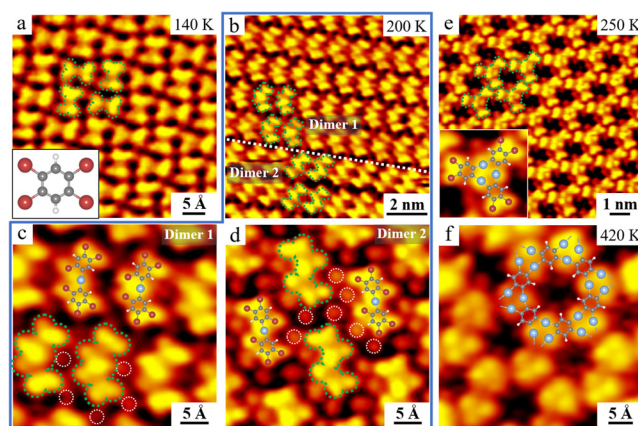


Fig. 3 Sequential debromination of 1,2,4,5-TBB on Ag(111). (a) STM image of intact 1,2,4,5-TBB molecules obtained upon deposition at ~ 140 K. (b) Large-scale STM image showing the coexistence of dimer 1 and dimer 2 in a molecular island after annealing at ~ 200 K, where the boundary is depicted by a dotted line. (c and d) Close-up STM images of (c) dimer 1 and (d) dimer 2, with the corresponding DFT models overlaid. (e) STM image of organometallic trimers obtained after annealing at ~ 250 K. Bottom left: zoomed-in STM image showing an individual trimer superimposed with the DFT model. (f) STM image of organometallic networks formed after complete debromination upon deposition onto Ag(111) held at ~ 420 K. Individual motifs involved in the debromination process are depicted by green contours. White circles indicate dissociated bromine atoms. Typical scanning conditions: $V_t = -900$ mV, $I_t = 0.80$ nA.

~ 200 K led to the formation of two types of dimers (*i.e.*, dimer 1 and dimer 2) coexisting with a clear boundary (*cf.* Fig. 3b). Close inspection of the magnified STM images (Fig. 3c and d) together with DFT calculations reveals that two kinds of organometallic dimers are involved, with one Ag atom connecting two sides in either cis or trans configuration, and one Br atom in each molecular component is eliminated. It is also noteworthy that metal atoms involved show bright contrasts similar to the cases

discussed above as well as reported previously,^{4,6} and both structural models match well with the corresponding STM morphologies. After further annealing the sample at ~250 K, islands of organometallic trimers were found (Fig. 3e), where individual ones could be identified as indicated by the green contours. As inspired by the previous studies^{4,12} and compared with STM observations,^{4,6} we attributed the three central bright protrusions to Ag atoms, connecting three neighboring dibrominated components. The large-scale STM images of islands composed of organometallic dimers and trimers are also provided in Fig. S5 (ESI†). Furthermore, when 1,2,4,5-TBB was deposited onto Ag(111) held at ~420 K, 2D organometallic networks appeared (Fig. 3f). The corresponding structural model is superimposed on the STM image with a good agreement. Therefore, 1,2,4,5-TBB also tends to debrominate step by step, generating organometallic dimers and trimers (with the removal of the first one and the neighboring one in each molecule), until the ultimate fabrication of a 2D organometallic network *via* complete debromination. Interestingly, *ortho*-dihalo-substitution, which is supposed to undergo [2+2] and [2+2+2] cycloaddition pathways^{4,30} to generate four- and six-membered carbon ring scaffolds, is found to gradually grow into 2D organometallic networks in this study.

Hence, by applying three typical symmetric polyhalogenated aromatics, a stepwise metal-mediated dehalogenation scenario was experimentally displayed, with the organometallic intermediates clearly visualized in real space. We propose that the sequential debromination should have a lower reaction barrier compared to that of the simultaneous dissociation of all Br atoms. Moreover, after Br dissociation, Ag adatoms could further stabilize the corresponding structures by forming organometallic intermediates (*e.g.*, organometallic dimers at <RT^d), and thus the sequential dehalogenation could be visualized.

In this work, multiple substitutions on a single benzene (including halogen substitution *ortho*, *meta*, and *para*) with different symmetries and their dehalogenation reaction processes have been experimentally investigated. A series of organometallic intermediates fabricated during sequential debromination processes of polybrominated benzenes were monitored on Ag(111). These results thus indicate a hierarchical debromination scenario of typical symmetric polybrominated aromatics, which would broaden the understanding of on-surface synthesis and expand the database of sequential debromination details.

The authors acknowledge financial support from the National Natural Science Foundation of China (Grants No. 22125203, 21790351 and 22202153) and the Fundamental Research Funds for the Central Universities (Grant No. 22120220051).

Conflicts of interest

There are no conflicts to declare.

Notes and references

- 1 S. Mondal, *ChemTexts*, 2016, **2**, 17.
- 2 C. Zhang, Z. Yi and W. Xu, *Mater. Futures*, 2022, **1**, 032301.
- 3 L. Gross, F. Mohn, N. Moll, P. Liljeroth and G. Meyer, *Science*, 2009, **325**, 1110–1114.
- 4 C. Zhang, E. Kazuma and Y. Kim, *Angew. Chem., Int. Ed.*, 2019, **58**, 17736–17744.
- 5 Q. Zhong, K. Niu, L. Chen, H. Zhang, D. Ebeling, J. Björk, K. Müllen, A. Schirmeisen and L. Chi, *J. Am. Chem. Soc.*, 2022, **144**, 8214–8222.
- 6 W. Gao, F. Kang, X. Qiu, Z. Yi, L. Shang, M. Liu, X. Qiu, Y. Luo and W. Xu, *ACS Nano*, 2022, **16**, 6578–6584.
- 7 S. W. Hla, L. Bartels, G. Meyer and K. H. Rieder, *Phys. Rev. Lett.*, 2000, **85**, 2777–2780.
- 8 P. Ruffieux, S. Wang, B. Yang, C. Sánchez-Sánchez, J. Liu, T. Dienel, L. Talirz, P. Shinde, C. A. Pignedoli, D. Passerone, T. Dumslaff, X. Feng, K. Müllen and R. Fasel, *Nature*, 2016, **531**, 489–492.
- 9 D. J. Rizzo, G. Veber, J. Jiang, R. McCurdy, T. Cao, C. Bronner, T. Chen, S. G. Louie, F. R. Fischer and M. F. Crommie, *Science*, 2020, **369**, 1597–1603.
- 10 Q. Fan, D. Martin-Jimenez, D. Ebeling, C. K. Krug, L. Brechmann, C. Kohlmeier, G. Hilt, W. Hieringer, A. Schirmeisen and J. M. Gottfried, *J. Am. Chem. Soc.*, 2019, **141**, 17713–17720.
- 11 S. Li, H. Yu, X. Chen, A. A. Gewirth, J. S. Moore and C. M. Schroeder, *Nano Lett.*, 2020, **20**, 5490–5495.
- 12 R. Zhang, B. Xia, H. Xu and N. Lin, *Angew. Chem., Int. Ed.*, 2019, **58**, 16485–16489.
- 13 M. Fritton, D. A. Duncan, P. S. Deimel, A. Rastgoo-Lahrood, F. Allegretti, J. V. Barth, W. M. Heckl, J. Björk and M. Lackinger, *J. Am. Chem. Soc.*, 2019, **141**, 4824–4832.
- 14 T. Wang, J. Huang, H. Lv, Q. Fan, L. Feng, Z. Tao, H. Ju, X. Wu, S. L. Tait and J. Zhu, *J. Am. Chem. Soc.*, 2018, **140**, 13421–13428.
- 15 J. Huang, Y. Pan, T. Wang, S. Cui, L. Feng, D. Han, W. Zhang, Z. Zeng, X. Li, P. Du, X. Wu and J. Zhu, *ACS Nano*, 2021, **15**, 4617–4626.
- 16 D. Y. Li, X. Qiu, S. W. Li, Y. T. Ren, Y. C. Zhu, C. H. Shu, X. Y. Hou, M. Liu, X. Q. Shi, X. Qiu and P. N. Liu, *J. Am. Chem. Soc.*, 2021, **143**, 12955–12960.
- 17 L. Hafferentz, V. Eberhardt, C. Dri, C. Africh, G. Comelli, F. Esch, S. Lecher and L. Grill, *Nat. Chem.*, 2012, **4**, 215–220.
- 18 Z. Zeng, D. Guo, T. Wang, Q. Chen, A. Matěj, J. Huang, D. Han, Q. Xu, A. Zhao, P. Jelinek, D. G. de Oteyza, J. S. McEwen and J. Zhu, *J. Am. Chem. Soc.*, 2022, **144**, 723–732.
- 19 C. X. Wang, J. L. Chen, C. H. Shu, K. J. Shi and P. N. Liu, *Phys. Chem. Chem. Phys.*, 2019, **21**, 13222–13229.
- 20 D. Han, Z. J. Tao, T. Wang, L. Feng, X. Y. Li, Z. W. Zeng and J. F. Zhu, *J. Phys. Chem. C*, 2022, **126**, 5541–5549.
- 21 T. Dienel, J. Gómez-Díaz, A. P. Seitsonen, R. Widmer, M. Iannuzzi, K. Radican, H. Sachdev, K. Müllen, J. Hutter and O. Gröning, *ACS Nano*, 2014, **8**, 6571–6579.
- 22 J. P. Hu, Z. F. Liang, K. C. Shen, L. Xie, H. Zhang, C. Q. Huang, Y. B. Huang, H. Huang, J. X. Tang, Z. Jiang, M. Yu and F. Song, *Nano Res.*, 2021, **14**, 4704–4713.
- 23 H. Lu, W. E. L. Cai, Z. Ma, W. Xu and X. Yang, *J. Phys. Chem. Lett.*, 2020, **11**, 1867–1872.
- 24 D. Sadowsky, K. McNeill and C. J. Cramer, *Environ. Sci. Technol.*, 2013, **47**, 14194–14203.
- 25 S. Li, S. Duan, Z. Zha, J. Pan, L. Sun, M. Liu, K. Deng, X. Xu and X. Qiu, *ACS Nano*, 2020, **14**, 6331–6338.
- 26 J. Shang, Y. Wang, M. Chen, J. Dai, X. Zhou, J. Kuttner, G. Hilt, X. Shao, J. M. Gottfried and K. Wu, *Nat. Chem.*, 2015, **7**, 389–393.
- 27 Q. Sun, X. Yu, M. Bao, M. Liu, J. Pan, Z. Zha, L. Cai, H. Ma, C. Yuan, X. Qiu and W. Xu, *Angew. Chem., Int. Ed.*, 2018, **57**, 4035–4038.
- 28 Q. Fan, T. Wang, L. Liu, J. Zhao, J. Zhu and J. M. Gottfried, *J. Chem. Phys.*, 2015, **142**, 101906.
- 29 X. Yu, L. Cai, M. Bao, Q. Sun, H. Ma, C. Yuan and W. Xu, *Chem. Commun.*, 2020, **56**, 1685–1688.
- 30 C. Sánchez-Sánchez, A. Nicolai, F. Rossel, J. Cai, J. Liu, X. Feng, K. Müllen, P. Ruffieux, R. Fasel and V. Meunier, *J. Am. Chem. Soc.*, 2017, **139**, 17617–17623.